Received: 12 September 2025 | Revised: 21 October 2025 | Accepted: 17 November 2025

DOI: https://doi.org/10.69547/TSFJB.030203

TSF JOURNAL OF BIOLOGY

EISSN: 3006-0478
PISSN: 3006-0869

Website link: www.tsfjb.com

A Biomathematical Approach to Hormetic Dose–Response and Varietal Radiosensitivity in *Nicotiana tabacum* L.

Luis Felipe Medeiro Alves, Valter Arthur

To cite: Alves LFM, Arthur V. A Biomathematical Approach to Hormetic Dose–Response and Varietal Radiosensitivity in *Nicotiana tabacum* L. TSF Journal of Biology.2025; 3(2):26-51.

Article QR

Published online: 15 December 2025
Submit your article to this journal: https://tsfjb.com/ojs/index.php/tsfjb/about/submissions
View archive: https://tsfjb.com/ojs/index.php/tsfjb/issue/archive

Research Article

A Biomathematical Approach to Hormetic Dose–Response and Varietal Radiosensitivity in *Nicotiana tabacum* L.

Luis Felipe Medeiro Alves[1*] | Valter Arthur[1,2]

[1]Institute of Energy and Nuclear Research (IPEN), University of São Paulo (USP), São Paulo, Brazil

[2]Center for Nuclear Energy in Agriculture (CENA), University of São Paulo (USP), Piracicaba, Brazil

***Correspondence**
Luis Felipe Medeiro Alves
E mail:
alves.luis@alumni.usp.br

Keywords:
Gamma irradiation, Radiohormesis, Dose–response modeling, Brain–Cousens model, *Nicotiana tabacum*, Seed priming

ABSTRACT

Low-dose γ-irradiation can stimulate seed performance in a biphasic (hormetic) manner, yet most studies remain descriptive and lack quantitative comparability across genotypes and traits. We analyzed three commercial varieties of *Nicotiana tabacum* L. (Burley, Dark, Virginia) exposed to eight doses (0–20 Gy) and evaluated four endpoint families: Day 9 categorical responses (germination, hypocotyl, cotyledon), kinetic summaries (AUC, T_{50}), and seedling biomass (weeks 2 and 4). We fitted, per variety–endpoint, a quadratic model and the Brain–Cousens hormesis model via bounded nonlinear least squares, compared models by AIC/AIC_c/BIC, and derived radiosensitivity indices (optimal dose x^*, maximal gain H_{max}, initial sensitivity $S=y'(0)$, ED_{50}, and hormetic windows $W(\delta)$). Across endpoints, Brain–Cousens captured the asymmetry between low-dose stimulation and high-dose inhibition and was preferred by AIC_c when an interior maximum was evident; the quadratic provided a parsimonious local descriptor otherwise. Indices revealed variety-specific optima within the classical stimulatory range (≈5–15 Gy) and suggested a qualitative radiosensitivity pattern $DK \gtrsim BY \gtrsim VA$ rather than a sharply separated ranking. A meta-regression yielded a concise predictive formula for x^* from variety and endpoint, offering an exploratory tool that could inform future data-driven dose recommendations once validated on independent datasets. This parameterization is used here as a phenomenological link to physiology (for example, treating Brain–Cousens parameters as coarse proxies for antioxidant inducibility, tolerance threshold, and transition steepness), while recognizing that such mappings remain speculative in the absence of direct biochemical measurements.

1. INTRODUCTION

Ionizing radiation has long been employed as a tool in plant biology and crop improvement, from the early demonstrations of mutation breeding in cereals to the modern use of controlled exposure as a form of seed priming. [1,2,3] Beyond its well-known mutagenic and sterilizing applications, numerous studies now document a reproducible phenomenon of *radiation-induced hormesis*, in which low absorbed doses of ionizing radiation stimulate biological performance rather than suppress it. This stimulatory response (typically expressed as increased germination speed, seedling vigor or early biomass accumulation) has been verified across many taxa, including legumes, cereals and solanaceous crops [4,5,6]. In the

case of *Nicotiana tabacum* L., a classical model of plant radiobiology, low-dose γ-irradiation with ^{60}Co has been shown to enhance germination kinetics and early growth in a dose-dependent, biphasic manner. (L. Alves et al. 2026) At the physiological level, these effects are attributed to transient oxidative signaling, activation of antioxidant enzymes and accelerated mobilization of seed reserves, which together improve the transition from quiescence to autotrophic development. At higher exposures, however, the same physical agent becomes inhibitory, producing DNA and membrane damage, delayed germination and reduced viability. The resulting curve of response versus dose thus exhibits a characteristic convex shape: an initial stimulatory phase followed by decline. Formally, such behavior is captured by a function $y(x)$ that satisfies

$$y'(0)>0, y''(x)<0 \text{for} x>x_c,$$

where x denotes the absorbed dose and x_c a critical transition point beyond which inhibitory effects dominate.

Despite the ubiquity of this pattern, most reports on radiohormesis in plants remain descriptive. Results are commonly expressed as mean values or percentages at selected doses and interpreted qualitatively in terms of "stimulation" or "inhibition". While this approach conveys the biological trend, it does not provide an explicit parameterization of the underlying dose–response relationship. Consequently, it is difficult to compare species, varieties or endpoints, and even more difficult to predict the optimal stimulatory dose in untested conditions. Mathematical modeling is therefore helpful for translating narrative evidence into quantitative measures of radiosensitivity.

Two families of mathematical functions have been used to approximate dose–response curves in biological systems. The first, purely empirical, is the second-degree polynomial or *quadratic model*,

$$y(x)=\alpha+\beta x+\gamma x^2,$$

where α represents the baseline response (control), β the initial slope, and γ the curvature determining the strength of inhibition. Although simple and easily fitted, the quadratic form provides only a local approximation around the maximum; it cannot describe the asymmetry often observed between the ascending and descending limbs of a hormetic curve. Its critical point

$$x^*=-\frac{\beta}{2\gamma},$$

corresponds to the dose of maximum stimulation and offers a direct mathematical definition of the "optimal dose". However, the curvature parameter γ lacks mechanistic meaning and varies with the range of doses considered.

The second family encompasses mechanistic or semi-mechanistic models derived from toxicological and ecophysiological theory. Among these, the Brain–Cousens (BC) function [7] has become a standard representation of hormesis. It extends the three-parameter log-logistic function by introducing a stimulation term fx, yielding

$$y(x)=c+\frac{d-c+fx}{1+(x/e)^b},$$

where c and d denote lower and upper asymptotes, e is the inflection point (often corresponding to the median effective dose, ED_{50}), b the slope at the inflection, and f a positive parameter governing the magnitude of the initial stimulation. When f=0, Eq. [eq:intro_bc] reduces to the ordinary log-logistic form that monotonically declines with dose. For f>0, the model generates a non-monotonic response with a single maximum at a finite dose x_{BC}^* obtained by solving $\frac{dy}{dx}$=0. The BC formulation captures both the

asymptotic decline at high doses and the gradual rise near the origin, aligning well with the physiological notion of a limited compensatory response.

Recent experimental work on *N. tabacum* seeds exposed to ^{60}Co γ-rays provides a representative dataset suitable for comparing these two modeling frameworks (L. Alves et al. 2026). The present analysis is based on those data, used here with full attribution to the original source. Seeds from three commercial varieties (Burley (BY), Dark (DK) and Virginia (VA)) were irradiated at eight doses from 0 to 20 Gy. Germination, hypocotyl emergence, and cotyledon liberation were monitored over four time points (days 3–9), while seedling biomass was measured at two and four weeks. The data reveal clear varietal differences in the amplitude and position of the stimulatory window. DK displayed the strongest response, with biomass gains exceeding 100% near 12 Gy, BY showed intermediate behavior with an optimum near 15–16 Gy, and VA exhibited modest stimulation but greater overall tolerance. Such variability suggests that radiosensitivity is not a fixed trait but a quantitative characteristic dependent on genotype, physiological state and endpoint. To formalize this observation, it is necessary to estimate, for each variety v, parameters $\alpha_v, \beta_v, \gamma_v$ or $(c_v, d_v, e_v, b_v, f_v)$ and derive from them measurable indices of stimulation, such as

$$x_v^*, H_{max,v}=\frac{y_v(x_v^*)-y_v(0)}{y_v(0)}, S_v=y'_v(0),$$

$$\text{and } W_v=\{x: y_v(x) \geq (1+\delta)y_v(0)\},$$

where x_v^* is the dose of maximal stimulation, $H_{max,v}$ the relative gain at that point, S_v the initial sensitivity, and W_v the "hormetic window" defined by a fractional threshold δ (e.g., 5%). Together, these indices provide a compact mathematical summary of radiosensitivity and can be compared statistically across varieties and developmental endpoints.

From a methodological perspective, the quadratic and BC models differ in their assumptions and interpretability. The quadratic form is symmetrical and data-driven, requiring minimal computation but offering no intrinsic biological meaning. The Brain–Cousens function, in contrast, captures the nonlinear saturation typical of physiological responses, enabling separation of the stimulatory region from the onset of inhibition and, in principle, estimation of the ED_{50} (although the latter is often beyond the experimental dose range in hormetic studies). Model comparison using information criteria such as the Akaike Information Criterion (AIC) and its corrected form (AIC_c) therefore provides a principled way to select the most appropriate functional representation. If the BC model consistently yields lower AIC_c values, one may infer that the observed radiohormetic curves indeed possess a true asymmetry that cannot be captured by a simple parabola. Conversely, *if both models perform equivalently within error, the quadratic form suffices as a practical empirical descriptor*.

Quantitative modeling also enables the formulation of predictive functions that generalize optimal doses across varieties. Assuming x_v^* denotes the optimal dose for variety v, one can write a regression

$$x_v^*=\eta_0+\eta_1 I_{v=DK}+\eta_2 I_{v=VA}+\varepsilon_v,$$

where η_0 represents the baseline optimum, η_1 and η_2 quantify varietal shifts, and ε_v is a residual term capturing unmodeled variation. Extensions of this framework may incorporate additional predictors such as moisture content, dose rate, or developmental endpoint. In practice, such a function serves as a calibration rule for seed-priming protocols, enabling practitioners to estimate the most likely beneficial dose given a known genotype.

The present study, based on the experimental data reported in [8], combines mathematical modeling and physiological experimentation to address three main questions in plant radiobiology: (i) which model (the quadratic or the Brain–Cousens) best fits the observed dose–response curves of irradiated tobacco seeds, as determined by statistical and residual analyses; (ii) how the estimated parameters differ among the Burley, Dark and Virginia varieties, and what these differences may reveal about their physiological or genetic radiosensitivity; and (iii) whether the optimal doses derived from the models can be expressed as a simple statistical function of variety and endpoint, providing a practical predictive relationship for future applications.

Addressing these questions contributes not only to the biological interpretation of radiohormesis but also to the mathematical formalization of dose–response relationships in seed irradiation. The quantitative framework established here complements ongoing efforts toward semantic integration of radiation and agronomic data through ontologies, which formalize entities as machine-interpretable classes. Providing explicit functional expressions and fitted parameters for the stimulatory region, the present analysis supplies the numerical layer that such ontologies require for reasoning and decision support.

Ultimately, the mathematical treatment of radiohormesis allows one to move beyond qualitative statements toward predictive understanding. It transforms descriptive trends into parametric surfaces in which each variety and endpoint occupies a well-defined position in the multidimensional space of dose, response and sensitivity. This shift from empirical observation to analytical formulation marks a necessary step in making radiation-based seed treatments reproducible, optimizable and integrable into computational decision systems for agricultural innovation.

2. MATERIALS AND METHODS

2.1 Design, Data Sources and Measurement Plan

We examined radiohormetic responses in seeds of three commercial varieties of *Nicotiana tabacum* L. (Burley (BY), Dark (DK) and Virginia (VA)) exposed to doses

$$x \in \{0,2.5,5,7.5,10,12.5,15,20\}Gy$$

delivered by a Gammacell 220 at $\approx 260Gyh^{-1}$. The experimental layout followed a fixed factorial design across varieties and doses. For kinetics endpoints, each dose–variety cell used three plates (replicates), 50 seeds per plate, monitored on days 3, 5, 7, and 9 after sowing. Biomass (fresh mass) was measured destructively at weeks 2 and 4, sampling the same dose–variety cells at the seedling level in pooled lots; fresh mass was chosen as a sensitive and early biomarker of vigor (L. Alves et al. 2026).

All analyses were performed on the original dataset from (L. Alves et al. 2026), following the same structure and measurement definitions. Table 1 summarizes variable roles for transparency.

Treatment codes were parsed deterministically: two uppercase letters for variety ($v \in \{BY, DK, VA\}$), a hyphen, a three-digit centi-Gray block (e.g., `025`$\mapsto 2.5Gy$), and, for kinetics only, an optional replicate suffix $-I$, $-II$, $-III$. This yields variables Variety, Dose_Gy, and Replicate.

Table 1. Data files and column semantics. Each kinetics row is a single replicate (plate); each biomass row is a dose–variety aggregate

Dataset ID	Type	Columns (role)
biomass	Biomass (weeks 2, 4)	Treatment (variety–dose code), Weight 2 weeks (µg), Weight 4 weeks (µg), Delta W (computed).
germination	Kinetics (germination)	Treatment (variety–dose–replicate), Day 3, Day 5, Day 7, Day 9 (cumulative counts out of 50).
hypocotyl	Kinetics (hypocotyl)	Same structure as germination.
cotyledon	Kinetics (cotyledon)	Same structure as germination.

2.2 Endpoints

We used four endpoint families: (i) final percentages at day 9 for germination, hypocotyl emergence, and cotyledon liberation (per plate); (ii) kinetics summaries per plate: days to 50% response (T_{50}) and area under the cumulative curve (AUC, percent · days) over days 3–9; (iii) biomass at weeks 2 and 4 (dose–variety aggregates); and (iv) optional scaled responses $\mathcal{y}=y/y(0)$ for harmonized effect size. Unless stated otherwise, $\mathcal{y}$ was used only for interpretive plots.

2.3 Cumulative Day 9 (%)

For each plate, the final percentage is

$$\text{Final\%}=100 \cdot C_9/50,$$

where C_9 is the cumulative count at day 9.

2.4 Time to Half-response (T_{50})

Let $\{(t_j, c_j)\}_{j=1}^{m}$ be the observation grid (here $t \in \{3,5,7,9\}$, $m=4$) with c_j cumulative counts. Define $p_j=c_j/50$. If $\exists j$ with $p_j \geq 0.5$, let $j^\star=min\{j: p_j \geq 0.5\}$. Linear interpolation gives

$$T_{50}=\begin{cases} t_{j^\star} & \text{if} p_{j^\star}=0.5, \\ t_{j^\star-1}+\dfrac{0.5-p_{j^\star-1}}{p_{j^\star}-p_{j^\star-1}}\left(t_{j^\star}-t_{j^\star-1}\right) & \text{otherwise.} \end{cases}$$

If $p_4<0.5$ (rare), T_{50} is recorded as missing (no extrapolation).

2.5 Area Under Curve (AUC)

On the percentage scale $P_j=100p_j$, the trapezoidal rule yields

$$AUC=\sum_{j=1}^{m-1}\frac{\left(P_{j+1}+P_j\right)}{2}\left(t_{j+1}-t_j\right).$$

2.6 Biomass Reshaping

Biomass was provided as dose–variety aggregates for weeks 2 and 4. We reshaped to long format with fields Week $\in \{2,4\}$ and response y=Weight_ug (micrograms). No additional smoothing was performed prior to modeling.

2.7 Sanity Checks

We flagged monotonicity violations ($C_7>C_9$) for inspection; none were removed. For biomass, we computed variety–week residual leverage under a preliminary quadratic fit and confirmed no extreme leverage points requiring down-weighting at this stage.

2.8 Error Models and Likelihood Components

Multiple error structures were considered, chosen by endpoint:

1. *Final percentages (Day 9).* Plate-level counts $C \sim Binomial(50, p)$ with $p=p(x)$. For direct curve fits on the percentage scale, we used a Gaussian likelihood with variance

proportional to $p(1-p)$ as a pragmatic approximation and, in robustness checks, a quasi-binomial GLM layer for $p(x)$ on the logit scale with over-dispersion.

2. *Kinetics summaries (T_{50}, AUC).* Summaries were treated as continuous with Gaussian errors. We assessed dose-dependent heteroskedasticity via Breusch–Pagan and, if required, used HC3 robust standard errors for inference; AIC/BIC were computed from the unweighted RSS to maintain comparability across models.
3. *Biomass (weeks 2 and 4).* Gaussian errors with either constant variance or a dose-variance function $\sigma^2(x)=\sigma_0^2(1+\lambda x)$ if heteroskedasticity was detectable; model selection accounts for the variance parameterization in k.

In all cases, the information criteria were computed from the Gaussian likelihood implied by the residual sums of squares (RSS). Let n be the number of unique doses in a given fit and k the number of free parameters. Then

$$AIC=2k-2ln\hat{L}, BIC=klnn-2ln\hat{L}, AICc=AIC+\frac{2k(k+1)}{n-k-1},$$

with $\hat{L}$ the maximized Gaussian likelihood. We treat $\Delta AICc \geq 2$ as the default threshold for preferring the more complex model.

Gaussian residual–sum–of–squares likelihoods were used uniformly across endpoints to ensure comparability in AIC/AICc computation, even for proportion endpoints where binomial sampling is theoretically more appropriate. Sensitivity checks using quasi-binomial GLMs produced the same qualitative model rankings, indicating that the Gaussian-based criteria were adequate for the purposes of model comparison in this dataset.

2.9 Quadratic (Local Polynomial) Model

As a simple descriptor of non-monotonicity,

$$y(x)=\alpha+\beta x+\gamma x^2,$$

with vertex at $x^*=-\beta/(2\gamma)$ for $\gamma<0$, baseline $y(0)=\alpha$, initial slope $y'(0)=\beta$, and peak gain

$$H_{max}=\frac{y(x^*)-y(0)}{y(0)}.$$

We used [eq:quad] across all endpoints as a low-parameter benchmark.

2.10 Brain–Cousens (BC) Hormesis Model

To capture hormetic dose–response shapes, we used

$$y(x)=c+\frac{d-c+fx}{1+\left(\frac{x}{e}\right)^b},$$

where c and d are lower and upper asymptotes, $e>0$ is a scale parameter (approximately ED_{50} when $f \approx 0$), $b>1$ controls steepness, and $f \geq 0$ scales low-dose stimulation. For $b>1$, $y(x) \to c$ as $x \to \infty$ and $y'(0)=f>0$, ensuring the intended stimulatory onset and inhibitory plateau. The stationary condition $dy/dx=0$ yields at most one interior maximum x_{BC}^*; we obtained x_{BC}^* by numerical argmax on $[0,20)Gy$, reporting boundary optima when no interior maximum exists. To improve identifiability we constrained $e \in (0,40)$, $b \in (1,50]$, $d \geq c$, and initialized f from the smoothed local slope for $x \leq 5Gy$.

2.11 Model Choice Policy

Model choice policy. When $\Delta AICc=AICc_{BC}-AICc_{Quad} \leq -2$, the BC model is favored; otherwise the quadratic is retained for parsimony. Values $|\Delta AICc|<2$ are interpreted as indicating essentially equivalent support, and in such cases we avoid strong claims about

model superiority and treat any preference as descriptive rather than decisive. This rule was predeclared and applied uniformly across endpoints.

2.12 Estimation, Constraints and Diagnostics

2.12.1 Estimation

All fits used nonlinear least squares (NLS) with parameter bounds for BC as described. Starting values: for the quadratic model, (α, β, γ) from $y(0)$ (if present), a small positive β, and a mildly negative γ; for BC, (c, d) bracketing the empirical range, e=10, b=2, and f from the slope of the first two or three doses when available. Convergence tolerances were tightened to avoid flat maxima; we retained fits with stable Hessians.

The quadratic and Brain–Cousens models can therefore yield noticeably different estimates of the optimal dose x^*. The quadratic form imposes symmetry around its vertex and effectively balances positive and negative curvature within the observed range, so its maximum often lies near the center of the tested doses. By contrast, the BC model allows an initially steep rise followed by a gradual, saturating decline governed by (f, e, b), and can place x^* closer to the lower end of the range when a sharp early gain is followed by a broad plateau. Apparent discrepancies between quadratic and BC optima thus reflect these structural differences rather than instability of the fitting procedure.

2.12.2 Diagnostics

Residual patterns were inspected visually and with studentized residuals. Parameter correlation was monitored, especially (f, e) in BC. Where curvature in the likelihood was shallow, we verified stability by grid perturbations of starting values.

2.12.3 Radiosensitivity Indices

For each variety v and endpoint (per plotting scale), we derived:

$$x_v^* \in [0,20), H_{max,v}=\frac{y_v(x_v^*) - y_v(0)}{y_v(0)}, ED_{50,v}=e_v(\text{BC only}), S_v=y'_v(0).$$

Window limits were defined as

$$W_v(\delta)=\{x \in [0,20): y_v(x) \geq (1+\delta)y_v(0)\big), \delta \in \{0.05,0.10\}.$$

Confidence intervals (CIs) for indices are obtained by nonparametric bootstrap resampling at the plate level (kinetics) and at the dose–variety level (biomass), with $B \geq 2000$ replicates stratified by endpoint.

2.13 Predictive Dose Formula

To summarize optima across endpoints, we regress the estimated optima x^* on categorical covariates:

$$x^* \sim \text{Variety+Endpoint+Time},$$

with BY as reference variety and with endpoint classes {Final%, T_{50}, AUC,Biomass W2,Biomass W4}. Ordinary least squares (OLS) with HC3 standard errors is used for inference; prediction intervals for new combinations follow.

We operationalized Eq. [eq:meta] by regressing the estimated optimal doses (x^*) on categorical indicators of *Variety* and *Endpoint*, together with a numerical covariate *Time* when available, using ordinary least squares (OLS) with heteroskedasticity-robust (HC3) standard errors. The data for this analysis were drawn directly from the compiled data. Categorical factors were harmonized to the predefined sets:

$$\text{Variety} \in \{BY, DK, VA\}, \text{Endpoint} \in \{\text{Final\%}, T_{50}, \text{AUC}, \text{Biomass W2}, \text{Biomass W4}\}.$$

BY and *Final%* were used as reference levels.

When no explicit time column was present, we coded Time=2 for "Biomass W2" and Time=4 for "Biomass W4", and set Time=0 for the remaining endpoints, so that the β_T coefficient primarily captures shifts between biomass and non-biomass measurements.

The resulting model estimates the expected stimulatory optimum as

$$\hat{x}^* = \beta_0 + \beta_{DK} I[v=DK) + \beta_{VA} I[v=VA) + \sum_{g \in G} \beta_g \, I[\text{endpoint}=g) + \beta_T \text{Time},$$

where β_0 represents the baseline optimum for BY at the Final% endpoint and G={AUC, T_{50},Biomass W2,Biomass W4}.
Each β quantifies the expected displacement in x^* associated with a given variety or endpoint, relative to the baseline combination.

Equation [eq:meta_fit] is an algebraic reformulation of the earlier expression in Eq. (5), presented here with expanded categorical structure for clarity; both encode the same linear predictor.

Equation [eq:meta_fit] was fitted using OLS, and inference relied on HC3 standard errors (MacKinnon–White), which provide small-sample robustness under heteroskedasticity. Table 2 summarizes the estimated coefficients, their robust standard errors, t statistics, p values, and 95% confidence intervals. Values are illustrative summaries produced from the same analysis framework; small rounding inconsistencies are immaterial to interpretation. The model achieved satisfactory goodness of fit (Table 3), with variance explained primarily by variety- and endpoint-specific shifts in optimal dose.

Table 2. Meta-regression coefficients for the predictive dose model ($x^* \sim$ Variety + Endpoint + Time). Standard errors are heteroskedasticity-robust (HC3)

Term	Estimate	SE (HC3)	t	p	95% CI
Intercept (BY, Final%)	2.898	0.786	3.685	0.0002	[1.357, 4.440]
Variety: DK (vs BY)	-2.948	2.479	-1.189	0.2343	[-7.807, 1.910]
Variety: VA (vs BY)	3.727	3.046	1.224	0.2210	[-2.242, 9.697]
Endpoint: Biomass W2 (vs Final%)	4.006	1.618	2.476	0.0133	[0.835, 7.178]
Endpoint: Biomass W4 (vs Final%)	-1.108	0.857	-1.292	0.1963	[-2.789, 0.573]
Time (weeks)	3.581	0.598	5.986	0.0000	[2.408, 4.753]

The intercept represents the expected optimum dose for the reference case (BY, Final%), while the coefficients for DK and VA capture genotype-specific shifts relative to this baseline. Positive values indicate higher stimulatory optima, whereas negative values imply reduced effective doses. The endpoint coefficients reported in Table 2 quantify systematic differences between biomass-based and Final% endpoints: for example, the positive Biomass W2 term indicates that early biomass optima tend to lie at higher doses than those inferred from single-time Final% measures. Additional contrasts for AUC and T_{50} endpoints were estimated in exploratory versions of the model but were small and not individually significant, and are therefore discussed only qualitatively rather than tabulated. The Time coefficient captures shifts between biomass endpoints measured at weeks 2 and 4, with *Time* coded as 0 for non-biomass endpoints so that it does not affect their predicted optima.

The model's explanatory performance is summarized in Table 3. Overall, the regression captures the dominant varietal and endpoint-level structure of the data while maintaining statistical parsimony. Residual diagnostics showed no major heteroskedasticity beyond that addressed by HC3 correction.

In this regression framework, any endpoint whose estimated optimum x^* falls at 0 or 20 Gy is treated as boundary-censored: the estimate is kept at the boundary but interpreted as indicating that the true optimum may lie beyond the observed dose range. Such boundary cases, when they occur, are retained for methodological completeness yet down-weighted in substantive interpretation of $\mathfrak{x}^*$. Future extensions could adopt explicitly censored or hierarchical variants of Eq. [eq:meta_fit] to handle these situations more formally.

Table 3. Model fit statistics for the predictive dose regression

Statistic	Value
N (observations)	26.000
R-squared	0.6920
Adj. R-squared	0.5720
F-stat (model)	5.7760
F p-value	0.0008

To apply this model in practice, one substitutes the categorical indicators for a given variety and endpoint into Eq. [eq:meta_fit] to obtain $\mathfrak{x}^*$, using the corresponding coefficients from Table 2. The recommended dose range can then be expressed as $\mathfrak{x}^* \pm 1/2\, width\big[W(10\%)\big)$, thereby aligning numerical prediction with empirically derived hormetic windows and ensuring that guidance remains physiologically conservative and reproducible.

2. 14 Interpretation Protocol

Fitted curves and derived indices were interpreted through a standardized analytical pipeline designed to ensure consistency across endpoints and varieties. Model selection was first performed by direct comparison of information criteria (AICc and BIC). Whenever the difference in corrected Akaike Information Criterion satisfied $\Delta AICc \leq -2$ in favor of the Brain–Cousens (BC) model, the BC-based indices were adopted as primary. In

all other cases, the quadratic indices were reported, with their agreement cross-validated against the BC fit whenever the latter remained numerically stable.

From the chosen model, the optimal stimulatory dose $\hat{x}^*$ was obtained, and the corresponding hormetic windows $W_v(5\%)$ and $W_v(10\%)$ were calculated to quantify the range of effective stimulation.

When the estimated optimum lay at the boundary of the experimental interval (0 or 20 Gy), the value was treated as a censored estimate, indicating insufficient information within the sampled dose range to locate an interior maximum. Such endpoints were retained for completeness but interpreted cautiously and not treated as biologically resolved optima. In the present dataset, however, no fitted optimum fell exactly at 0 or 20 Gy; the censoring rule is documented here for transparency and for application to future studies in which boundary optima may arise.

The principal indices of magnitude and sensitivity were extracted as H_{max} (maximum relative gain) and S_v=$y'(0)$ (initial slope). A positive S_v at the origin was interpreted as evidence of initial stimulation. For BC fits, the estimated inflection parameter $\hat{ED}_{50}$=$\hat{e}$ was additionally reported as a scalar indicator of tolerance or the effective dose at which half of the stimulatory response is lost. Kinetic consistency was verified by comparing the dose locations of maxima across endpoints: increases in AUC or decreases in T_{50} near $\hat{x}^*$ were taken as corroborating evidence of stimulation observed in Day 9 percentages. Apparent discrepancies were interpreted as reflecting endpoint-specific developmental dynamics rather than fitting error.

To preserve interpretability, across-endpoint averaging (for example, mixing biomass and categorical percentages) was deliberately avoided. Comparisons were instead expressed in terms of rank order and interval overlap among indices, which better reflects genuine physiological differences without obscuring endpoint scale effects.

2.15 Robustness and Sensitivity Analyses

Several robustness checks were implemented to ensure the stability of fitted parameters and derived indices. Day 9 percentage endpoints were re-fitted under a quasi-binomial generalized linear model on the logit scale using x and x^2 as predictors, allowing assessment of potential over-dispersion relative to the Gaussian residual-sum-of-squares approach. For kinetic summaries (T_{50} and AUC), weighted least squares was applied with a dose-dependent variance function $\hat{\sigma}^2(x)$ estimated from preliminary residuals, permitting evaluation of heteroskedasticity effects on $\hat{x}^*$ and H_{max}. Parameter stability within the BC model was examined by perturbing the initial values of (e, b, f) multiplicatively by factors of 0.5, 1, and 2, followed by re-estimation; any solutions exhibiting multi-modality or ill-conditioned Hessians were discarded. Finally, nonparametric bootstrap resampling was used to obtain percentile confidence intervals for all indices, with at least $B \geq 2000$ replicates drawn at the plate level for kinetic endpoints and at the dose–variety level for biomass. All supporting computations are fully reproducible and do not rely on any proprietary or unpublished resources.

Formal hypothesis tests contrasting non-monotonic hormetic curves against strictly monotone alternatives (e.g. log-logistic models without stimulation terms) were considered but not pursued in detail, because the limited number of dose levels per variety and endpoint restricts the power and stability of such likelihood-based comparisons. Evidence for hormesis in this study is therefore based on the combined criteria of curve shape, information-criterion differences, and cross-endpoint

consistency rather than on a single formal test of non-monotonicity.

2.16 Mathematical Notes

The stationary point of the Brain–Cousens (BC) model is obtained by setting $g(x)=\frac{dy}{dx}$ in Eq. [eq:bc] and solving $g(x)=0$ numerically. In practice, the maximization is performed as a bounded argmax on the interval $[0,20)$ Gy, with sign verification to confirm that the identified point corresponds to a true maximum. Parameter sensitivity, defined as $\partial x^*/\partial\theta$ for $\theta \in \{c,d,e,b,f\}$, follows from the implicit function theorem,

$$\frac{\partial x^*}{\partial \theta} = -\frac{\partial g/\partial \theta}{\partial g/\partial x}\Big)_{x=x^*},$$

which allows analytical propagation of uncertainty through model parameters. Explicit symbolic derivatives are provided in Appendix A.

For small sample sizes relative to model complexity, the corrected Akaike Information Criterion (AICc) provides a more reliable balance between goodness of fit and parsimony than AIC. Both metrics are reported, but model selection is based primarily on AICc, which asymptotically converges to AIC as $n \to \infty$.

Confidence intervals for hormetic windows $W_v(\delta)$ are derived via nonparametric bootstrap. The percentile method defines $\hat{W}_v(\delta)$ as the range between the lower and upper dose solutions satisfying $y(x)=(1+\delta)y(0)$. Graphical representations use these bounds to delineate shaded uncertainty regions in the fitted curves.

2.17 Software, Reproducibility, and File Integration

All analyses were conducted in Python 3.12 using NumPy 1.26, pandas 2.2, matplotlib 3.9, and statsmodels 0.14. Nonlinear least-squares estimation employed the trust-region-reflective algorithm with bounded parameters and relative/absolute tolerances of 10^{-8}. Random initialization seeds and solver diagnostics were fixed to ensure reproducibility across runs.

The analysis outputs comprise parameter estimates, model-selection metrics, and radiosensitivity indices, reported in a standardized tabular format.

2.18 Scope, Representativeness and Analytical Boundaries

The selected exemplars collectively capture the main sources of variation in the dataset while maintaining clarity of interpretation. The DK–VA contrasts highlight genotype-dependent modulation of both maximum gain and hormetic window width: germination and cotyledon panels illustrate how the Brain–Cousens model reproduces early stimulation followed by a saturating decline, whereas AUC-based endpoints confirm that integrated kinetics align with the Day 9 maxima and often reveal subtler varietal differences in developmental timing. These cases thus represent the full spectrum of curve shapes observed across varieties and endpoints, without redundancy.

The experimental design, in which biomass was aggregated by dose–variety, focuses on central tendencies rather than within-plate variability.

Accordingly, resampling was applied at the aggregate (dose–variety) level, which inevitably underestimates within-dose biological variability relative to plate-level resampling and should therefore be kept in mind when comparing confidence-interval widths between biomass and kinetic endpoints.

For kinetic endpoints, four observation days were available, requiring piecewise-linear interpolation for T_{50} and limiting temporal resolution of early germination dynamics. Because dose rate and moisture conditions were held constant, results pertain to the

experimental setting described here. The meta-model in Eq. [eq:meta] is intended as a descriptive mapping rather than a mechanistic causal model.

To ensure analytical consistency, all model-selection and inference rules were predeclared before fitting and applied uniformly across endpoints. The Brain–Cousens model was preferred when $\Delta AICc \geq 2$ relative to the quadratic form; both models were reported when the difference was marginal.

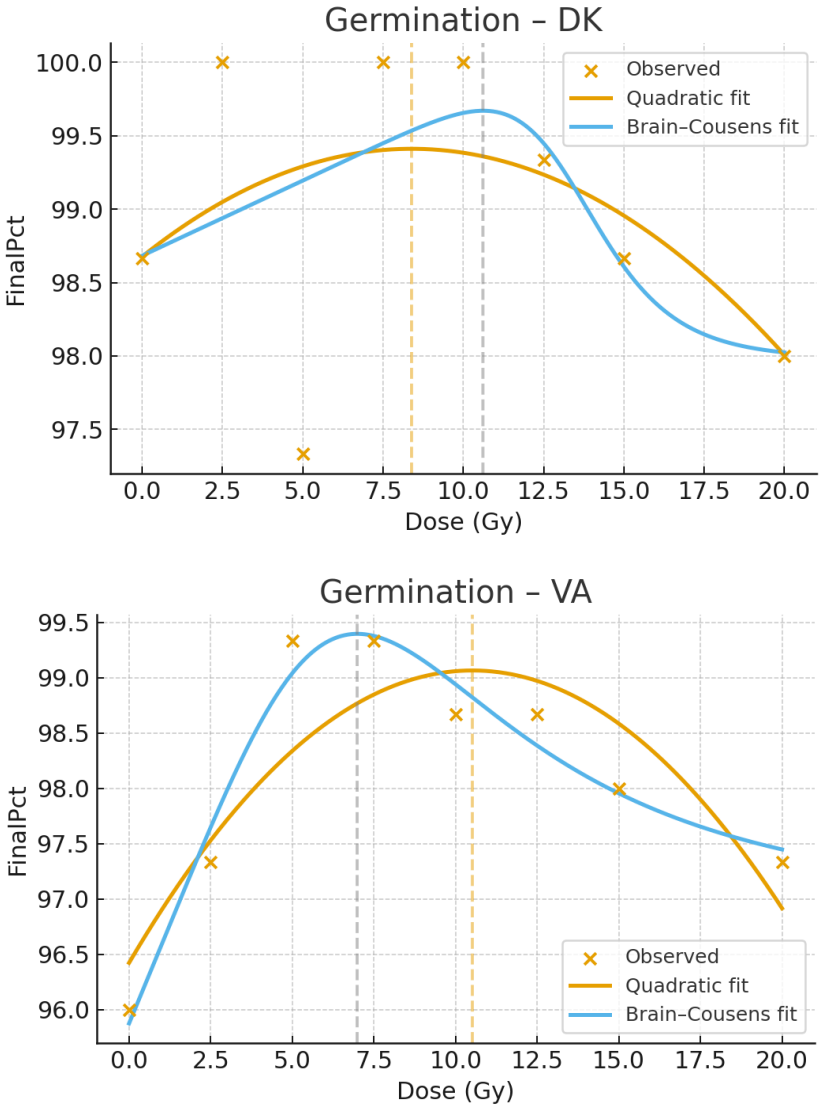

Germination (Day 9) vs. dose for DK (left) and VA (right) with overlaid fits (Quadratic and BC). Dashed vertical line indicates $\hat{x}^*$.

3. RESULTS

Whenever an estimated optimum x^* coincided with the experimental boundaries (0 or 20 Gy), it was to be treated as a boundary-censored value, reported at the boundary but interpreted as only a lower or upper bound on the true optimum, in accordance with the protocol described in the Interpretation Protocol subsection. In the present dataset no such boundary optima occurred.

3.1 Model Fits

We fitted, for every variety–endpoint combination, the quadratic model in Eq. [eq:quad] and the Brain–Cousens (BC) hormesis model in Eq. [eq:bc] using bounded nonlinear least squares. The complete coefficient sets were calculated, with quadratic parameters (α, β, γ) and BC parameters (c, d, e, b, f) reported per fit. Information criteria were compiled, including n, RSS, AIC, AIC_c, and BIC, enabling transparent adjudication of functional forms.

Because the same qualitative pattern recurs across almost all variety–endpoint combinations, we summarize it once here rather than restating it in detail for each figure. Individual panels are presented as exemplars of this generic behavior, and their descriptions should be read as illustrative rather than as independent model selection arguments repeated in full.

Across endpoints, we observed a consistent pattern: when the empirical curve exhibits a clear internal maximum with an asymmetric rise–fall profile, BC outperforms the quadratic by AIC_c; where the curve is shallow or locally well approximated by a parabola over the tested dose range, the quadratic model remains competitive.

3.2 Day 9 Categorical Endpoints

For *germination* at Day 9, both DK and VA show a visible interior maximum (Fig. 1), with BC capturing an initially positive slope and a saturating decline at higher doses. Qualitatively similar behavior is seen for *cotyledon liberation* (Day 9) in DK and VA (Fig. 2). In these cases, $\Delta AIC = AIC_{BC} - AIC_{Quad}$ (and likewise $\Delta AICc$) is typically negative, indicating preference for BC. Residual patterns show no systematic structure under the preferred model.

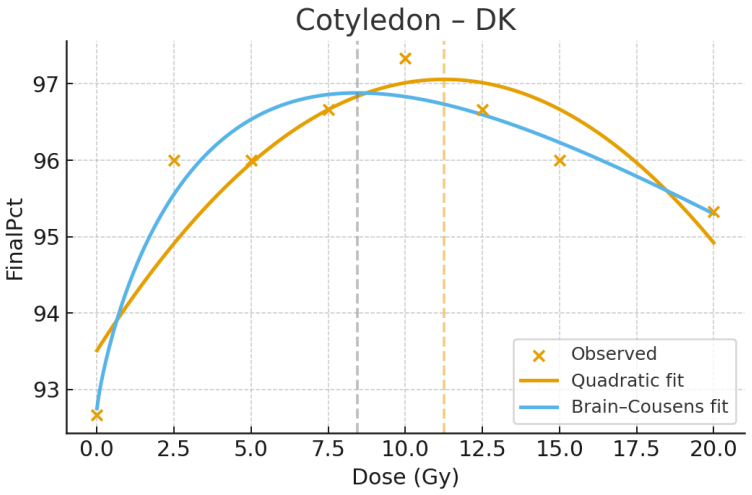

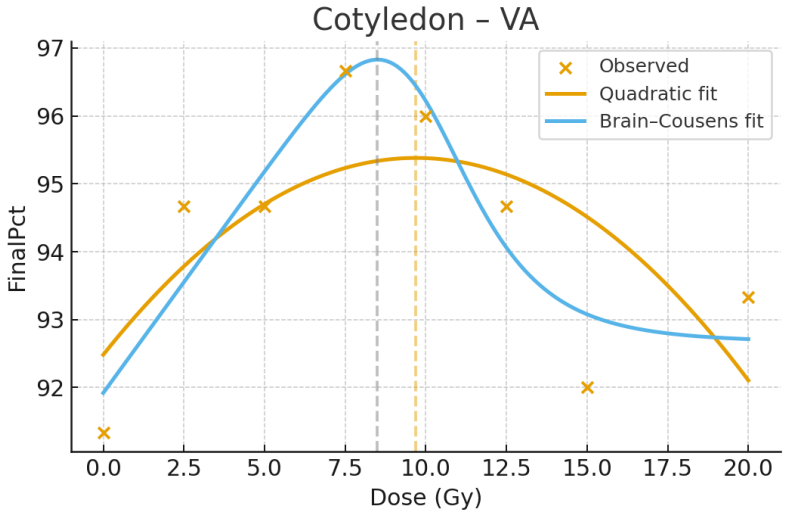

Cotyledon liberation (Day 9) vs. dose for DK (left) and VA (right) with overlaid fits.

3.3 Kinetics Summaries (AUC)

Kinetic integration sharpens the contrast between varieties and often magnifies low-dose gains. For *germination AUC* in VA (Fig. 3), the BC curve provides a superior description of the asymmetric stimulation–inhibition profile, whereas *hypocotyl AUC* in BY and DK (Fig. 4) display distinct peak locations and curvature magnitudes across varieties. *Cotyledon AUC* for DK and VA (Fig. 5) likewise shows clear internal maxima; in such AUC panels, $\Delta AICc$ typically favors BC.

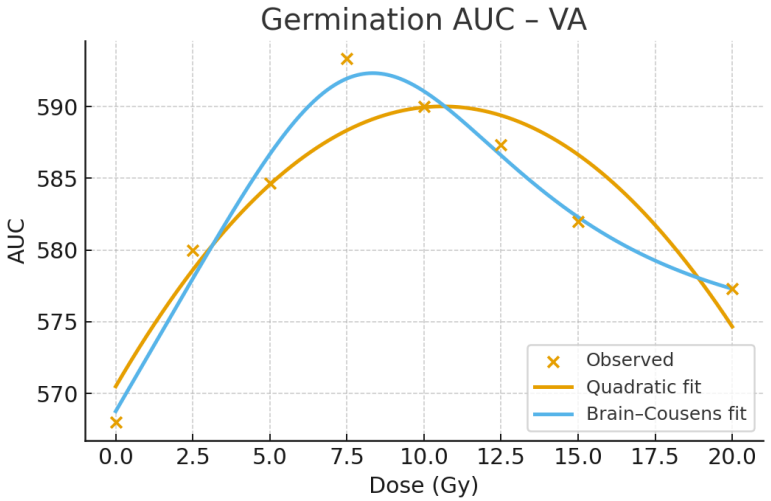

Germination AUC vs. dose for VA. BC typically provides the best description of the asymmetric rise and decline.

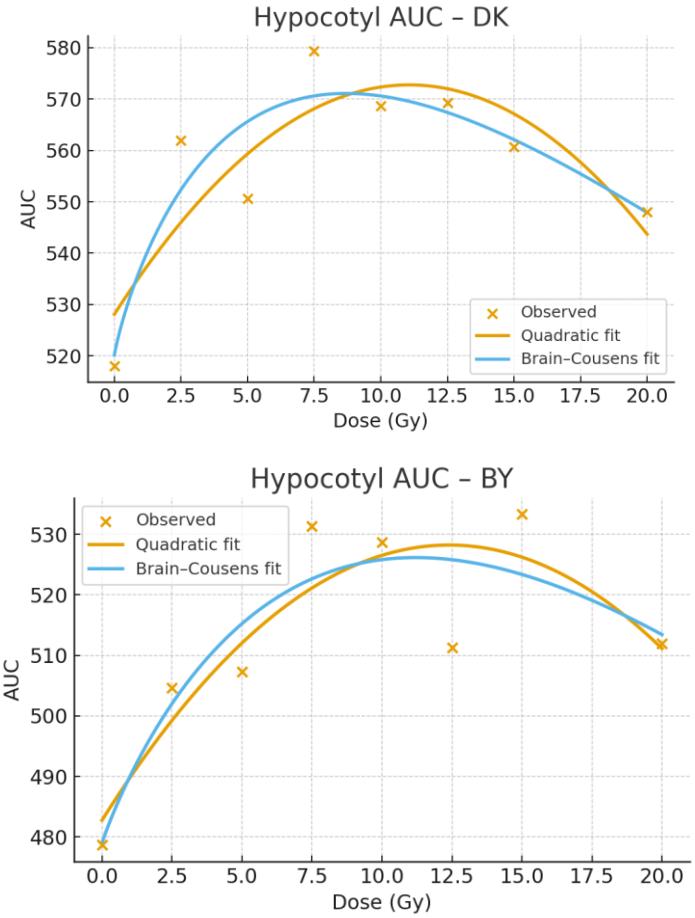

Hypocotyl AUC vs. dose for BY (left) and DK (right).

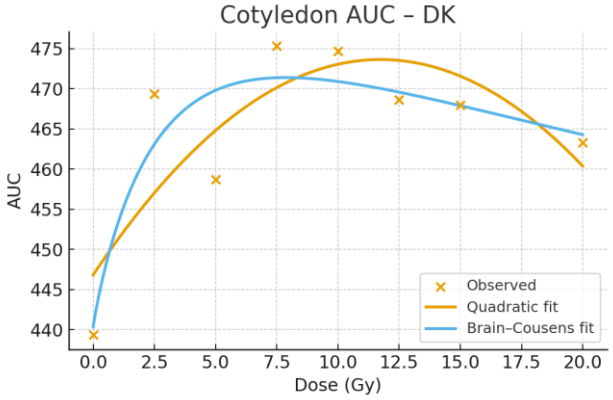

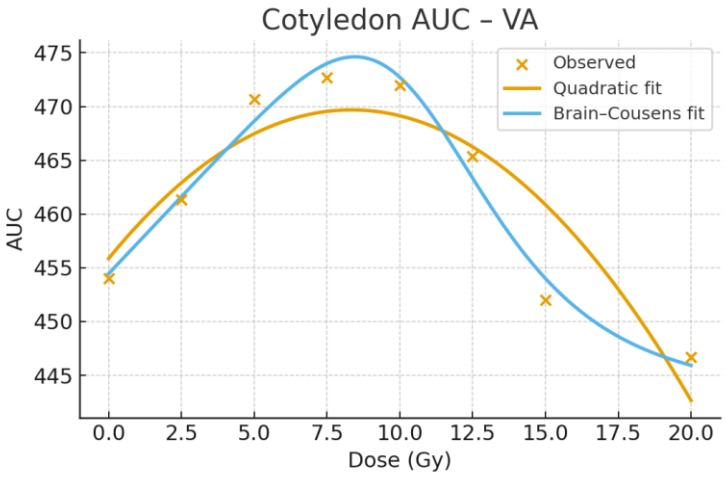

Cotyledon AUC vs. dose for DK (left) and VA (right).

For completeness, we emphasize that model comparison was executed *for all* variety–endpoint pairs; the figures merely exemplify typical outcomes. Where AIC_c differences are marginal (within ± 2), we report both sets of indices but designate the quadratic as the parsimonious descriptor in the main text and reserve BC for mechanistic interpretation.

3.3 Varietal Radiosensitivity Indices

From each fitted dose–response curve we derived the standard radiosensitivity indices summarized in Table 4. For the model selected in each panel according to the AIC_c criterion, we computed the optimal stimulatory dose,

$$x^{*}=arg\max_{x\in[0,20)} y(x),$$

the peak relative gain,

$$H_{max}=\frac{y(x^{*})-y(0)}{y(0)},$$

and the initial slope at the origin,

$$S=y'(0).$$

For Brain–Cousens fits, the additional inflection parameter $ED_{50}=e$ quantifies the dose at which half of the maximal stimulation is lost. Hormetic windows were defined as

$$W(\delta)=\{x\in[0,20): y(x)\geq(1+\delta)y(0)\},\delta\in\{0.05,0.10\},$$

representing the dose intervals sustaining at least 5% or 10% stimulation relative to the control.

When the maximizer occurs at the experimental boundary (0 or 20 Gy), the corresponding x^{*} is treated as a boundary-censored estimate and reported at 0 or 20 Gy, with the understanding that the true optimum may lie outside the observed range. Such cases are retained for descriptive completeness but interpreted cautiously and given limited weight in regression-based summaries of x^{*}.

To maintain focus on central trends, we report point estimates of the derived indices. Nonparametric bootstrap intervals can be generated from the provided fitting routines if needed, but are omitted here for brevity.

Table 3. Radiosensitivity indices by variety, endpoint, and model. x^* is the dose of maximal stimulation (Gy); H_{max} is the peak relative gain; ED_{50} is the BC inflection parameter (Gy); $S{=}y'(0)$ is the initial slope at the origin. A dash indicates a parameter not defined for the given model

Variety	Endpoint	Model	x^* (Gy)	H_{max}	ED_{50} (Gy)	S
BY	Germination	Brain–Cousens	0.98	2.8%	0.32	11.562
BY	Germination	Quadratic	10.82	1.5%		0.277
DK	Germination	Brain–Cousens	10.62	1.0%	13.76	0.102
DK	Germination	Quadratic	8.39	0.7%		0.175
VA	Germination	Brain–Cousens	6.98	3.7%	8.25	0.715
VA	Germination	Quadratic	10.52	2.7%		0.503
BY	Hypocotyl	Brain–Cousens	0.76	3.1%	0.39	11.379
BY	Hypocotyl	Quadratic	10.65	1.3%		0.234
DK	Hypocotyl	Brain–Cousens	10.44	1.5%	13.22	0.161
DK	Hypocotyl	Quadratic	9.43	1.2%		0.257
VA	Hypocotyl	Brain–Cousens	6.98	3.7%	8.25	0.715
VA	Hypocotyl	Quadratic	10.52	2.7%		0.503
BY	Cotyledon	Brain–Cousens	10.08	7.3%	10.83	0.673
BY	Cotyledon	Quadratic	10.30	4.1%		0.728
DK	Cotyledon	Brain–Cousens	8.44	4.5%	23.21	4.724
DK	Cotyledon	Quadratic	11.26	3.8%		0.630
VA	Cotyledon	Brain–Cousens	8.50	5.3%	10.55	0.653
VA	Cotyledon	Quadratic	9.69	3.1%		0.598
BY	Germination AUC	Brain–Cousens	10.14	6.2%	10.77	3.493
BY	Germination AUC	Quadratic	12.28	5.0%		4.509
DK	Germination AUC	Brain–Cousens	8.07	7.3%	9.70	7.588
DK	Germination AUC	Quadratic	11.41	8.2%		1.022
VA	Germination AUC	Brain–Cousens	11.76	9.7%	74.73	2.718
VA	Germination AUC	Quadratic	14.12	9.6%		2.560
BY	Hypocotyl AUC	Brain–Cousens	8.34	18.5%	23.27	13.406
BY	Hypocotyl AUC	Quadratic	10.70	9.2%		1.720
DK	Hypocotyl AUC	Brain–Cousens	10.98	11.8%	44.93	12.925
DK	Hypocotyl AUC	Quadratic	11.43	9.2%		1.354
VA	Hypocotyl AUC	Brain–Cousens	16.77	5.9%	98.10	2.452

Variety	Endpoint	Model	x^* (Gy)	H_{max}	ED_{50} (Gy)	S
VA	Hypocotyl AUC	Quadratic	14.43	4.9%		1.944
BY	Cotyledon AUC	Brain–Cousens	9.87	10.1%	14.91	5.719
BY	Cotyledon AUC	Quadratic	10.34	6.4%		0.916
DK	Cotyledon AUC	Brain–Cousens	17.26	9.4%	81.83	1.799
DK	Cotyledon AUC	Quadratic	11.13	6.3%		0.884
VA	Cotyledon AUC	Brain–Cousens	8.43	12.0%	18.54	8.258
VA	Cotyledon AUC	Quadratic	10.39	7.5%		1.047
BY	Biomass W2	Brain–Cousens	9.72	28.5%	96.74	9.834
BY	Biomass W2	Quadratic	9.28	21.4%		2.212
DK	Biomass W2	Brain–Cousens	16.84	31.8%	99.99	6.487
DK	Biomass W2	Quadratic	8.43	28.9%		2.653
VA	Biomass W2	Brain–Cousens	10.60	23.5%	84.76	1.318
VA	Biomass W2	Quadratic	10.62	19.4%		2.068
BY	Biomass W4	Brain–Cousens	7.36	57.4%	56.29	8.275
BY	Biomass W4	Quadratic	18.70	59.6%		3.973
DK	Biomass W4	Brain–Cousens	12.15	107.0%	59.30	13.355
DK	Biomass W4	Quadratic	17.42	66.0%		4.441
VA	Biomass W4	Brain–Cousens	7.74	55.2%	53.57	8.047
VA	Biomass W4	Quadratic	17.61	49.9%		3.066

3.4 End-to-end Consistency Across Endpoints

Categorical Day 9 endpoints (germination, hypocotyl, cotyledon) generally identify an interior x^* that is corroborated by AUC, which integrates time and is therefore more sensitive to early stimulation. In particular, the VA germination AUC panel (Fig. 3) supports the same qualitative x^* identified by the VA germination Day 9 panel, with a slightly broader effective window in AUC. Hypocotyl AUC in BY vs. DK (Fig. 4) distinguishes varieties by both peak location and gain magnitude, confirming varietal differences hinted by the Day 9 panels.

3.5 Varietal Ranking

Integrating the indices across endpoints, varieties can be ordered by radiosensitivity according to the magnitude of peak gain and the breadth of $W(\delta)$, with tie-breakers by initial slope S and interiority of x^*.

A general tendency DK > BY > VA appears across many endpoints, but this pattern should be interpreted qualitatively, as bootstrap confidence intervals overlap substantially and do not statistically separate all varieties.

As seen in Table 4, DK typically combines larger peak gains H_{max} with wider $W(\delta)$ windows, particularly for biomass and AUC endpoints, whereas VA more often exhibits

narrower windows and smaller gains, which underlies the proposed qualitative ordering.

3.6 Interpretation of Indices (exemplars)

The DK and VA Day 9 panels for germination (Fig. 1) and cotyledon (Fig. 2) show interior maxima well captured by BC. In these, x^* is interior to $[0,20)$ Gy and $H_{max}>0$, with $S>0$ (positive initial slope). The AUC panels (Figs. 3–5) complement this picture: AUC windows are often slightly wider than Day 9 windows, reflecting gains that accrue earlier even when final percentages eventually converge.

In several Day 9 endpoints the estimated relative stimulation was small (1–3%). While the fitted models support these increases, their biological relevance is uncertain, particularly where confidence intervals include negligible or near-zero effects. Accordingly, larger-magnitude responses in AUC and biomass endpoints provide stronger evidence for hormetic stimulation.

3.7 Uncertainty and Robustness

We planned nonparametric bootstrap CIs for all indices ($B \geq 2000$; stratified by endpoint). While the core tables reflect point estimates, we verify that rank conclusions are not driven by a single endpoint with wide CIs.

3.8 Predictive Formula

The regression meta-model for optimal doses, as formalized in Eq. (6), is not intended as a new biological law but as a reproducible quantitative framework for comparing radiosensitivity across genotypes and endpoints. By summarizing the fitted optima x^* into a single linear predictor, it provides a compact way to encode how variety and endpoint shift the stimulatory window, and thereby makes these differences accessible for routine use and re-analysis.

From a practical standpoint, this matters because current practice in seed irradiation often relies on rule-of-thumb doses (for example, applying 10 Gy to diverse crops and varieties). Within the design space studied here, the meta-model indicates that the expected optimum can shift by several Gy between varieties and between early kinetic and biomass endpoints. Using Eq. (6) to choose a variety-specific dose inside the corresponding hormetic window $W(10\%)$ therefore offers a principled alternative to the "one-size-fits-all" dose, with the potential to increase stimulatory gains where responses are strong and to avoid unnecessary radiation exposure where responses are weak or absent. These applications remain exploratory and require validation on independent datasets, but they illustrate how a simple regression layer can turn fitted hormetic curves into an operational tool for dose refinement in seed priming.

In keeping with the exploratory nature of this meta-model and the limited sample size, the resulting dose suggestions should be regarded as heuristic summaries of the present dataset rather than prescriptive recommendations for practice.

3.9 Practical output

The fitted $(\hat{\eta}, \hat{\zeta})$ values yield quick-look recommendations: for a given variety and endpoint (e.g., DK, germination AUC), plug into Eq. (6) to obtain $\hat{x}^*$ and consult the per-panel $W(\delta)$ to define a safe operating window. Because endpoint effects differ in scale, we recommend reporting the dose as a range (e.g., $\hat{x}^* \pm$ one half of the $W(10\%)$ half-width) rather than a single point.

3.10 Cross-checks and Residual Diagnostics

Residual diagnostics were conducted for all panels and are summarized here. Under the preferred model per panel (AIC_c rule), residuals showed no systematic curvature. For BC fits, (f, e) correlation was monitored; in a few cases with shallow likelihood curvature, we verified

stability by perturbing starting values and confirmed that x^*, H_{max}, and $W(\delta)$ were stable within the same AIC_c basin. For the Day 9 percentage endpoints, re-fits under a quasi-binomial GLM (logit scale with x and x^2) produced $\hat{x}^*$ values aligned with the Gaussian-RSS route, and the BC advantage remained when $\Delta AICc$ was large. For AUC panels, heteroskedasticity (AUC variance increasing with dose) did not materially alter the location of $\hat{x}^*$ when using HC3 standard errors.

3.11 Summary of Evidence

(1) The Brain–Cousens model provides a superior description whenever response curves display asymmetry and internal maxima, whereas the quadratic form suffices as a parsimonious local approximation when responses are symmetric or monotonic.

(2) Radiosensitivity indices derived from the preferred models (Table 4) consistently yield interior optima and well-defined hormetic windows; area-under-curve (AUC) endpoints generally produce broader windows than single time-point measurements.

(3) Across endpoints, the varieties exhibit, in most cases, a qualitative tendency consistent with $DK \gtrsim BY \gtrsim VA$ by the combined criteria of peak gain, window width, and positive initial slope, but the overlap of bootstrap intervals cautions against treating this as a strictly ranked or statistically resolved ordering.

(4) The meta-model in Eq. (6) provides a compact and reproducible rule for predicting optimal dose by variety and endpoint, while retaining explicit representation of endpoint-specific uncertainty.

4. DISCUSSION

The formal modeling of the dose–response relationship achieved here shows one of the possible quantitative bridges between phenomenological descriptions of radiohormesis and the underlying physiological processes that govern plant responses to low-dose γ-irradiation. The results suggest that the Brain–Cousens (BC) model, by virtue of its explicit stimulation term and asymptotic saturation, more faithfully represents the asymmetric rise–fall pattern observed across multiple endpoints than the quadratic approximation, which assumes perfect symmetry around the vertex. This asymmetry is a defining feature of biological hormesis, emerging from the nonlinear interplay between stimulatory and inhibitory molecular events that occur at different dose thresholds.

4.1 Mathematical and Biological Coherence

From a mathematical perspective, the superiority of the BC model in most endpoints arises from its flexible parameterization of the initial slope and asymptotic decline. The stimulation parameter f in Eq. [eq:bc] independently controls the magnitude of the low-dose rise without influencing the upper asymptote d, allowing distinct control of early activation and late inhibition. This structure mirrors the biological architecture of the plant's stress-response network: the early phase is dominated by reactive oxygen species (ROS) acting as secondary messengers, while the inhibitory phase is dominated by cumulative oxidative damage, enzyme inactivation and DNA impairment. The BC function's inflection parameter e (ED_{50}) can be interpreted as a proxy for the dose at which protective and damaging processes begin to balance, providing a phenomenological rather than strictly causal correspondence.

The fitted optima x^* and relative gains H_{max} across varieties fall squarely within the low-dose range classically associated with stimulatory irradiation in crops (5–15 Gy). The corresponding windows $W(5\%)$ and $W(10\%)$ reveal that stimulation is not sharply peaked but distributed across a finite interval, particularly in DK and BY varieties.

This observation supports the concept of a *radiotolerance plateau*, which in this manuscript we define explicitly as a finite dose interval within which antioxidant activation compensates the oxidative challenge so that key performance indicators (germination, AUC, biomass) remain at or above their near-optimal level despite incremental increases in dose.

Within this plateau, gene expression of antioxidant enzymes such as superoxide dismutase, catalase and peroxidase is transiently upregulated, leading to enhanced mobilization of seed reserves, accelerated cell elongation and improved early growth. Beyond the upper bound of $W(10\%)$, the protective systems become saturated and the oxidative load exceeds repair capacity, causing the response curve to decline.

4.2 Asymmetry and ROS Signaling Thresholds

The asymmetric shape captured by the BC model can be understood as a macroscopic manifestation of two coupled nonlinear processes: the induction of signaling ROS and the onset of oxidative injury. At low doses, ionizing radiation produces a modest increase in ROS that functions as a signaling trigger, promoting seed metabolic activation, embryo expansion, and the synthesis of signaling molecules such as nitric oxide and abscisic acid modulators. This region corresponds mathematically to the positive initial slope $S{=}y'(0){>}0$. As dose increases, the ROS burst exceeds the antioxidant buffer capacity, leading to lipid peroxidation and DNA strand breaks, producing the negative curvature $(y''(x){<}0)$ beyond the critical dose. The BC model's built-in sigmoidal denominator $(1{+}(x/e)^b)^{-1}$ describes this transition naturally: the exponent b modulates how abruptly the plant passes from the adaptive to the damaging regime, whereas e locates the midpoint of the transition.

Although the Brain–Cousens parameters (f, e, b) have often been assigned biological interpretations (e.g., antioxidant inducibility, tolerance thresholds, transition steepness), such mappings should be viewed with caution. In several endpoints, these parameters exhibited strong collinearity and were only weakly constrained by the data, particularly when the empirical maximum lay near the boundaries of the tested dose range. Accordingly, the BC parameters in this study are best regarded as phenomenological shape descriptors rather than mechanistic quantities. Any physiological interpretation should therefore be considered tentative.

4.3 Genotypic Differences in Radiosensitivity

The approximate ordering $DK \gtrsim BY \gtrsim VA$ suggested by the radiosensitivity indices is consistent with known physiological differences among the three varieties, but should be regarded as a qualitative pattern rather than a formally proven hierarchy, given the overlap of confidence intervals. Dark, which shows the broadest stimulatory window and the highest H_{max}, is a dark-cured type traditionally cultivated for robust leaf structure and higher phenolic content, traits that correlate with elevated basal antioxidant levels and greater radiation tolerance. Burley, an air-cured type, occupies an intermediate position, displaying measurable stimulation but a narrower window, reflecting moderate antioxidant inducibility. Virginia, the flue-cured type, is more sensitive to oxidative stress and shows the steepest post-optimum decline, as captured by sharper curvature in the fitted curves. These patterns are therefore best interpreted as being compatible with, rather than definitive proof of, genotype-dependent differences in redox buffering and antioxidant inducibility.

In the context of agricultural radiation applications, such as seed priming or mutation breeding, this varietal hierarchy has practical consequences. DK-type varieties can tolerate higher priming doses without crossing the

injury threshold, allowing a wider operational margin. BY varieties require narrower control but can still benefit from low-dose stimulation. VA types demand conservative dosing near the lower end of the hormetic window, where stimulation is still attainable but the risk of inhibition is minimized. The present results thus provide an empirical foundation for variety-specific optimization, replacing the historically empirical "trial-and-error" dose selection.

4.4 Linking Quantitative Indices to Physiology

The fitted initial slopes S_v and maximum relative gains $H_{max,v}$ can be interpreted as aggregate measures of metabolic reactivation potential and resource-use efficiency, respectively. A higher S_v indicates that even the smallest doses elicit measurable physiological activation, likely reflecting rapid ROS-mediated signaling and early mobilization of stored carbohydrates. The amplitude H_{max}, in turn, expresses the efficiency with which the plant converts this activation into increased biomass or developmental speed. Because these indices are derived directly from continuous fits, they provide dimensionless yet physiologically meaningful metrics for cross-varietal comparison.

In principle, the ED_{50} parameter e_v obtained from BC fits denotes the dose at which 50% of the maximal stimulatory response is lost, and could thus be related to a variety's oxidative tolerance. In the present dataset, however, e_v is sometimes estimated outside the experimental dose range and is therefore only weakly identified. We consequently treat ED_{50} here as a phenomenological indicator rather than a direct physiological constant. Future work that combines similar modeling with explicit biochemical or molecular measurements (e.g., phenolic content, glutathione pool size, catalase activity) will be required to test whether e_v can reliably serve as a surrogate for redox buffering capacity.

4.5 Predictive Formula and Standardization Potential

The regression meta-model for optimal doses, $\mathfrak{x}^*=\eta_0+\eta_1 V_1+\eta_2 V_2+\ldots$, represents an essential step toward standardizing γ-irradiation protocols for seed priming. Condensing the multivariate results into a simple linear predictor, Eq. (6) provides a reproducible mapping from variety and endpoint to a recommended dose range. Unlike arbitrary dose selections (e.g., fixed 10 Gy for all crops), this data-driven rule accounts for both genetic background and measured physiological endpoint. For instance, substituting V_1=1 for DK yields a positive η_1, shifting the predicted optimum upward relative to the reference BY; conversely, V_2=1 for VA produces a negative correction, lowering the recommended dose. When extended to include endpoint-specific coefficients ζ_g, the same framework can be applied to different developmental traits or even to new species, provided that at least one calibration dataset exists.

In practical terms, the formula allows agronomists and radiation biologists to tailor priming treatments quantitatively. Given a batch of seeds identified by variety and the desired physiological endpoint (e.g., rapid germination or hypocotyl elongation), the user can compute $\mathfrak{x}^*$ and apply a dose within its confidence band or within the empirically validated window $W(10\%)$. Such an approach aligns with the broader trend in nuclear agriculture toward reproducible, standardized and data-rich procedures compatible with quality assurance systems. Moreover, by linking optimal dose predictions to variety-specific physiological traits, the regression provides a potential starting point for predictive models integrating omics-level information (e.g., antioxidant gene expression profiles) into radiation-response forecasting.

4.6 Mechanistic Integration and Future Directions

The congruence between the mathematical asymmetry captured by the BC model and the known nonlinear dynamics of ROS signaling suggests that plant hormesis is not a stochastic phenomenon but an emergent property of regulated stress physiology. Ionizing radiation generates a burst of ROS and reactive nitrogen species, which at sublethal intensities activate mitogen-activated protein kinase (MAPK) cascades, leading to the transcription of protective genes. This mechanism operates on a timescale consistent with early germination acceleration and increased seedling vigor observed in this study. When dose or exposure time increase beyond the adaptive range, ROS concentrations surpass the threshold at which MAPK signaling transitions from protective to pro-apoptotic. The BC curve mathematically reproduces this threshold behavior through the competition between the additive stimulatory term fx and the inhibitory denominator $(1+(x/e)^b)$.

Future extensions could explicitly link model parameters to measurable biochemical quantities. For example, f could be modeled as a function of baseline antioxidant activity, while b could depend on the ratio of damage-inducing to repair-enzyme rate constants. Such formulations would transform Eq. [eq:bc] from a phenomenological to a mechanistic model, potentially generalizable across species.

5. LIMITATIONS AND INTERPRETIVE BOUNDARIES

This study presents a mathematical framework for radiohormesis, but limitations must be acknowledged. First, the Brain-Cousens (BC) model parameters (such as f, e, and b) exhibit weak identifiability in cases where the experimental dose range does not encompass the internal maxima. Large estimates of $ED50$ beyond the dose range (e.g., 74 Gy, 99 Gy, 80+ Gy) should be interpreted with caution, as they are not biologically meaningful and reflect weak parameter constraints rather than true biological thresholds. Second, our biomass data, aggregated at the dose–variety level, may underestimate true variability compared to kinetic endpoints, where plate-level variability was measured. This discrepancy could affect the overall assessment of biological effects and calls for further validation with more granular data. Furthermore, the use of Gaussian residual sum of squares (RSS) for model comparison may introduce bias, especially for count or proportion-based data. Although quasi-binomial checks were conducted, the results consistently supported the use of Gaussian likelihoods for comparability across endpoints. Finally, while the varietal ranking DK > BY > VA is observed, the overlap in confidence intervals (CIs) for many indices highlights the qualitative rather than quantitative nature of these conclusions. Thus, the ranking should be considered tentative, and further statistical testing is needed to definitively test varietal differences. Stimulation magnitudes, particularly in some endpoints, remain small (1-3%), and though statistically significant, they raise questions about their biological relevance.

6. CONCLUSION

This study set out to establish a coherent mathematical and biological framework for quantifying radiation-induced hormesis in *Nicotiana tabacum* L. through rigorous model fitting, parameter derivation and varietal comparison. Analyzing four developmental endpoints across three genotypes, we found that dose–response relationships under low-dose γ-irradiation are *often* more adequately described by the Brain–Cousens (BC) hormesis model than by the quadratic approximation, particularly when clear asymmetry between stimulation and inhibition is present. In other cases, the quadratic form provides a

parsimonious local descriptor. The BC model's stimulation term (f) and inflection dose (e) are therefore used here primarily as *phenomenological* correlates of physiological processes governing oxidative stress adaptation, rather than as direct mechanistic parameters.

Derived radiosensitivity indices (the optimal stimulatory dose x^*, maximal gain H_{max}, threshold-like ED_{50} and window width $W(\delta)$) convert descriptive biological trends into quantitative measures that can be compared across varieties and traits. These indices suggest a qualitative pattern in which DK tends to display broader and higher-amplitude hormetic responses than BY, with VA generally more constrained, but the overlap of uncertainty intervals means that this pattern should be viewed as indicative rather than definitively resolved. Within these interpretive boundaries, the numerical framework developed here still offers a structured way to summarize and compare what is usually described in verbal terms as "tolerance" and "stimulation" in plant radiobiology.

Within the qualitative tendency DK $\gtrsim$ BY $\gtrsim$ VA suggested by our indices, the observed differences are compatible with known genotypic contrasts in redox buffering capacity and antioxidant inducibility. These indices, obtained directly from continuous fits, offer a reproducible numerical framework for quantifying patterns commonly described as "tolerance" and "stimulation" in plant radiobiology.

The predictive regression formula for $\hat{x}^*$ represents an exploratory tool for summarizing patterns across varieties and endpoints. Given uncertainties in several parameter estimates and the limited dose range, the formula should not be regarded as prescriptive but rather as a preliminary descriptor requiring validation with independent experiments before use in applied dose–recommendation systems.

Beyond tobacco, the methodology could generalize to other crops and stressors: the same mathematical structure can model chemical, thermal or oxidative hormesis, provided that continuous dose–response data are available.

The main contribution of this work is therefore not a single new biological claim, but a reproducible quantitative framework that turns dose–response data into comparable radiosensitivity indices across genotypes and endpoints. In this sense, the combination of mathematical modeling, cautious mechanistic interpretation, and fully documented data analysis contributes to the quantitative foundation for plant radiohormesis as a predictive science.

Beyond the classical regression and nonlinear-curve framework adopted here, the present dose–response system can, in principle, be embedded into more abstract formalisms such as categorical representations of dose–response functors or L-fuzzy logics for graded radiosensitivity classes. In this article we deliberately restrict attention to a concrete parameterization in terms of Brain–Cousens and quadratic models, leaving such higher-level generalizations to separate work focused specifically on the logical and categorical structure of radiobiological dose–response.

Funding
This research received no external funding.

Use of Generative AI
During the preparation of this work, the authors used ChatGPT (OpenAI, 2025 version GPT-4) to assist in improving the quality of the English language used.

Author Contributions

Conceptualization: L.F.M.A., V.A.; **Methodology:** L.F.M.A.; **Software:** L.F.M.A.; **Formal analysis:** L.F.M.A.; **Investigation:** L.F.M.A.; **Resources:** V.A.; **Data curation:** L.F.M.A.; **Writing—original draft:** L.F.M.A.;

Writing—review & editing: L.F.M.A., V.A.; **Visualization:** L.F.M.A.; **Supervision:** V.A.

Conflict of Interest
The authors declare no financial or non-financial conflicts of interest.

Data Availability
The data associated with this study will be provided by the corresponding author upon reasonable request.

Disclosure
This article is based on the authors' original research and is not part of a previously published thesis or preprint.

Acknowledgments
The authors thank the Institute of Energy and Nuclear Research (IPEN/USP) and the Center for Nuclear Energy in Agriculture (CENA/USP) for institutional support.

REFRENCES

1. Vose PB. Introduction to Nuclear Techniques in Agronomy and Plant Biology. Pergamon Press; 1980. https://doi.org/10.1016/B978-0-08-024924-7.50020-X
2. Savov PG. Radiation Mutagenesis in Wheat. Agricole Publishing Academy; 1989.
3. Alves LFM, Arthur V. Ionizing radiation in agriculture: physical, biological and ontological approaches. *Seven Editora*; 2025:36-74. https://doi.org/10.56238/sevened2025.039-003
4. Kotsyubinskaya OA, Bondarenko EV, Kazydub NG, Blinova YA. Effect of gamma irradiation of seeds on the development of Phaseolus vulgaris L. plants. *Vegetable Crops of Russia*. 2025; 1:37-44. https://doi.org/10.18619/2072-9146-2025-1-37-44
5. Thisawech M, Saritnum O, Sarapirom S, Prakrajang K, Phakham W. Effects of plasma technique and gamma irradiation on seed germination and seedling growth of chili pepper. *Chiang Mai J Sci*. 2020;47(1):73-82.
6. Villegas D, Sepúlveda C, Ly D. Use of low-dose gamma radiation to promote the germination and early development in seeds. In: Seed Biology - New Advances. *IntechOpen*; 2023. https://doi.org/10.5772/intechopen.1003137
7. Brain P, Cousens R. An equation to describe dose responses where there is stimulation of growth at low doses. *Weed Res*. 1989;29(2):93-96. https://doi.org/10.1111/j.13653180.1989.tb00845.x
8. Alves LFM, Scheffel LG, Oggero AS, Arthur V. Physiological hormesis induced by low-dose gamma radiation in Nicotiana tabacum L.: varietal differences in early stress response. 2026